Reconstruction of inclusions in photothermal imaging

A Carpio[1] **and ML Rapun**[2]

[1] *Universidad Complutense, Spain*

[2] *Universidad Politécnica de Madrid, Spain*

E-mail: carpio@mat.ucm.es

Abstract: Photothermal imaging allows to inspect the structure of composite materials by means of nondestructive tests. The surface of a medium is heated at a number of locations. The resulting temperature field is recorded on the same surface. Thermal waves are strongly damped. Robust schemes are needed to reconstruct the structure of the medium from the decaying time dependent temperature field. The inverse problem is formulated as a weighted optimization problem with a time dependent constraint. The inclusions buried in the medium and their material constants are the design variables. We propose an approximation scheme in two steps. First, Laplace transforms are used to generate an approximate optimization problem with a small number of stationary constraints. Then, we implement a descent strategy alternating topological derivative techniques to reconstruct the geometry of inclusions with gradient methods to identify their material parameters. Numerical simulations assess the effectivity of the technique.

Keywords: phototermal imaging, topological derivatives, gradient methods, constrained optimization

1 Introduction

Photothermal imaging has arisen as an effective tool for nondestructive testing of composite materials. The surface of a semi-infinite medium is heated with a laser beam. The temperature is then measured at a number of receptors placed on the surface during a time interval, see Fig. 1. This technique has been employed in recent experiments by [1, 2]. Here, we develop a theoretical framework to process the measured data and reconstruct the structure of inclusions buried in the medium.

The imaging set-up is depicted in Fig. 1. Let κ_e be the thermal conductivity of the exterior medium and ρ_e the density multiplied by its specific heat. Inclusions with thermal parameters κ_i and ρ_i are buried in it. The inverse problem consists in finding the inclusions Ω and their material parameters κ_i, ρ_i such that the temperature field measured at the detector locations $\mathbf{x}_1, \ldots, \mathbf{x}_M \in \Pi$ at times $t_1, \ldots, t_N$ agrees with the solution of the corresponding forward problem. This is a transmission problem for the heat equation governing the temperature field

$$U(\mathbf{x}, t) := \begin{cases} U_e(\mathbf{x}, t), & \text{in } \Omega_e \times (0, \infty) := (\mathbb{R}^2_- \setminus \Omega) \times (0, \infty), \\ U_i(\mathbf{x}, t), & \text{in } \Omega \times (0, \infty), \end{cases}$$

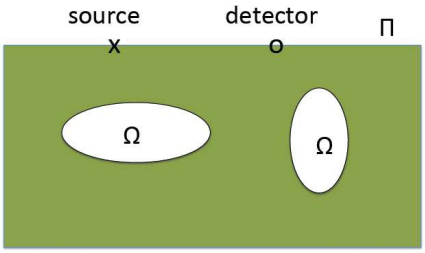

Figure 1. *Imaging set-up. Receptors and thermal sources are located on the boundary* Π *of the medium. The inclusions* Ω *and their material parameters must be reconstructed.*

given by

$$\begin{cases} \rho_e \partial_t U_e - \kappa_e \Delta U_e = 0, & \text{in } \Omega_e \times (0,\infty), \\ \rho_i \partial_t U_i - \kappa_i \Delta U_i = 0, & \text{in } \Omega \times (0,\infty), \\ U_i - U_e = U_{inc}, & \text{on } \partial\Omega \times (0,\infty), \\ \kappa_i \partial_{\mathbf{n}} U_i - \kappa_e \partial_{\mathbf{n}} U_e = \kappa_e \partial_{\mathbf{n}} U_{inc}, & \text{on } \partial\Omega \times (0,\infty), \\ \partial_{\mathbf{n}} U_e = 0, & \text{on } \Pi \times (0,\infty), \\ U_e(\mathbf{x},0) = U_i(\mathbf{x},0) = 0, & \forall \mathbf{x} \in \mathbb{R}^2_-, \end{cases} \tag{1}$$

where $\mathbb{R}^2_- := \{(x,y) \in \mathbb{R}^2,\ y < 0\}$ and $\Pi := \{(x,0),\ x \in \mathbb{R}\}$. The surface of the sample Π is thermically excited at a source point $\mathbf{x}_0 \in \Pi$ with a delta–pulse source, producing a thermal wave

$$U_{inc}(\mathbf{x},t) = \frac{1}{t} \exp\left(-\frac{\rho_e |\mathbf{x}-\mathbf{x}_0|^2}{4\kappa_e t}\right), \qquad \mathbf{x} \in \mathbb{R}^2,\ t > 0. \tag{2}$$

Adiabatic boundary conditions are imposed on the upper boundary Π.

The inverse problem is regularized using a constrained variational reformulation: Determine regions Ω and parameters κ_i, ρ_i minimizing the functional

$$J(\mathbb{R}^2_- \setminus \Omega, \kappa_i, \rho_i) = \frac{1}{2} \sum_{k=1}^{M} \sum_{j=1}^{N} f(t_j) \left(U_{total}(\mathbf{x}_k, t_j) - U_{meas}(\mathbf{x}_k, t_j)\right)^2, \tag{3}$$

where U_{total} is the solution of the time dependent forward problem (1) for an inclusion Ω with thermal parameters κ_i and ρ_i. The forward problem acts as a constraint. The weight function $f(t)$ normalizes the time decay of solutions of the heat equation:

$$f(t) = \max_{\mathbf{x} \in \{\mathbf{x}_1, \ldots, \mathbf{x}_M\}} |U_{meas}(\mathbf{x},t)|^{-1}.$$

Thermal waves are strongly damped. Time dependent weights prevent losing information as time grows.

2 Approximation using Laplace transforms

The time dependent heat problem can be efficiently solved combining Laplace transforms and stationary boundary element formulations. This suggests an alternative approximate variational formulation for the inverse problem, involving a small number of stationary constraints.

For each value of s, the Laplace transform of U

$$u_s(\mathbf{x}) = \int_0^\infty e^{-st} U(\mathbf{x},t) dt,$$

is a solution of a Helmholtz transmission problem with complex wave numbers depending on the parameter s [3]:

$$\begin{cases} \kappa_e \Delta u_s - s\rho_e u_s = 0, \quad \text{in } \Omega_e, \\ u_s^- - u_s^+ = u_{inc,s}, \quad \text{on } \partial\Omega, \\ \partial_{\mathbf{n}} u_s = 0, \quad \text{on } \Pi, \end{cases} \qquad \begin{cases} \kappa_i \Delta u_s - s\rho_i u_s = 0, \quad \text{in } \Omega, \\ \kappa_i \partial_{\mathbf{n}} u_s^- - \kappa_e \partial_{\mathbf{n}} u_s^+ = \kappa_e \partial_{\mathbf{n}} u_{inc,s}, \quad \text{on } \partial\Omega, \end{cases} \tag{4}$$

where $u_{inc,s} = \int_0^\infty e^{-st} U_{inc}(\mathbf{x}, t)dt$. The Laplace transform is then inverted choosing hyperbolic paths [4]: $\gamma(\theta) := \mu(1 - \sin(\pi/4 + \imath\theta))$, $\theta \in \mathbb{R}$, where $\mu > 0$. The solution of (1) takes the form

$$U(\mathbf{x}, t) = \frac{1}{2\pi\imath} \int_{-\infty}^{\infty} e^{t\gamma(\theta)} u_{\gamma(\theta)}(\mathbf{x})\gamma'(\theta)d\theta.$$

A truncated trapezoidal rule yields an approximation of U:

$$U(\mathbf{x}, t) \approx \sum_{\ell=-L}^{L} c_\ell e^{ts_\ell} u_{s_\ell}(\mathbf{x})$$

with nodes and weights:

$$s_\ell = \gamma\left(\frac{\log(L)}{L}\,\ell\right), \qquad c_\ell = \frac{\log(L)}{2\pi\imath L}\gamma'\left(\frac{\log(L)}{L}\ell\right).$$

As in [5, 6], we replace the original cost functional (3) by the approximate functional

$$J(\mathbb{R}^2_- \setminus \Omega, \kappa_i, \rho_i) = \frac{1}{2}\sum_{k=1}^{M}\sum_{j=1}^{N} f(t_j)\left(\sum_{\ell=-L}^{L} c_\ell e^{t_j s_\ell} u_{s_\ell}(\mathbf{x}_k) - U_{meas}(\mathbf{x}_k, t_j)\right)^2, \tag{5}$$

involving now $2L + 1$ stationary constraints: the Helmholtz transmission problems for the coefficient functions $u_{s_\ell}(\mathbf{x})$, $\ell = -L, ..., L$.

3 Descent strategy with respect to inclusions and parameters

To approximate solutions of the optimization problem we resort to a descent technique. Sequences of approximate inclusions and parameters are generated along which the cost functional (5) decreases. Descent with respect of the domains is implemented using topological derivatives. Descent directions for the parameters are determined using gradient methods.

Let us fix an initial guess of the parameters $\kappa_i = \kappa_i^0$ and $\rho_i = \rho_i^0$. A first guess of the inclusions is obtained calculating the topological derivative of the resulting shape functional.

The topological derivative $D_T(\mathbf{x}, \mathcal{R})$ of a shape functional $\mathcal{J}(\mathcal{R})$ is a scalar function of $\mathbf{x} \in \mathcal{R}$ that provides asymptotic expansions of the form [7]:

$$\mathcal{J}(\mathcal{R} \setminus B_\varepsilon(\mathbf{x})) = \mathcal{J}(\mathcal{R}) + D_T(\mathbf{x}, \mathcal{R})\pi\varepsilon^2 + o(\varepsilon^2), \quad \text{as} \quad \varepsilon \to 0.$$

Placing small inclusions $B_\varepsilon(\mathbf{x}) = B(\mathbf{x}, \varepsilon)$ at the points $\mathbf{x} \in \mathcal{R}$ where the topological derivative is negative the value of the functional decreases. Points where the topological derivative attains the largest negative values are likely to belong to inclusions of different materials. A first approximation Ω_1 of Ω is defined as the set of all the points where the topological derivative of $J(\mathbb{R}^2_-, \kappa_i^0, \rho_i^0)$ falls below a negative threshold (see [5, 8] for guidelines of the selection of such constant).

The evaluation of the topological derivative is effectively performed exploring explicit expressions in terms of forward and adjoint fields. Similarly to Theorem 3.2 in [5] we can prove

Theorem. *Fixing κ_i, ρ_i, the topological derivative of the functional $J(\mathbb{R}^2_- \setminus \Omega, \kappa_i, \rho_i)$ defined in (5) is*

$$D_T(\mathbf{x}) = Re\left(\sum_{\ell=-L}^{L} \frac{2\kappa_e(\kappa_e - \kappa_i)}{\kappa_e + \kappa_i}\nabla u_{total,s_\ell}(\mathbf{x})\nabla p_{s_\ell}(\mathbf{x}) + (\rho_e - \rho_i)s_\ell u_{total,s_\ell}(\mathbf{x})p_{s_\ell}(\mathbf{x})\right) \tag{6}$$

when $\mathbf{x} \in \mathbb{R}^2_- \setminus \Omega$, where $u_{total,s_\ell} = u_{inc,s_\ell} + u_{s_\ell}$, and u_{s_ℓ} is a solution of (4) for $s = s_\ell$. The fields p_{s_ℓ} are solutions of adjoint problems:

$$\begin{cases} \kappa_e\Delta p_{s_\ell} - s_\ell\rho_e p_{s_\ell} = g_{s_\ell}, \quad in\ \Omega_e, \\ p^-_{s_\ell} - p^+_{s_\ell} = 0, \quad on\ \partial\Omega \\ \partial_{\mathbf{n}} p_{s_\ell} = 0, \quad on\ \Pi, \end{cases} \qquad \begin{cases} \kappa_i\Delta p_{s_\ell} - s_\ell\rho_i p_{s_\ell} = 0, \quad in\ \Omega, \\ \kappa_i\partial_{\mathbf{n}} p^-_{s_\ell} - \kappa_e\partial_{\mathbf{n}} p^+_{s_\ell} = 0, \quad on\ \partial\Omega, \end{cases} \tag{7}$$

where $g_{s_\ell}(\mathbf{x}) := \sum_{i=1}^{M}\sum_{j=1}^{N} f(t_j)c_{s_\ell}e^{t_j s_\ell}\left(\overline{U_{meas}(\mathbf{x}_i,t_j) - \sum_{k=-L}^{L} c_k e^{t_j s_k} u_{s_k}(\mathbf{x}_i)}\right)\delta_{\mathbf{x}_i}(\mathbf{x})$.

To determine Ω_1, we set $\Omega = \emptyset$, $\kappa_i = \kappa_i^0$, $\rho_i = \rho_i^0$. Given an approximation Ω_d for fixed κ_i, ρ_i, a better one can be determined computing the topological derivative of $J(\mathbb{R}^2_- \setminus \Omega_d, \kappa_i, \rho_i)$ and adding to Ω_d points where it falls below a negative threshold.

Once a first approximation of the inclusion Ω_1 is selected, the parameters are updated using correctors provided by a gradient method. Given approximations $\kappa_i^{q-1}, \rho_i^{q-1}$ of the material parameters, we define $\kappa_i^q = \kappa_i^{q-1} + \eta\phi^q$ and $\rho_i^q = \rho_i^{q-1} + \eta\psi^q$, for small $\eta > 0$. The numbers ϕ^q, ψ^q are selected differentiating

$$J(\eta) := J(\Omega_i^0, \kappa_i^{q-1} + \eta\phi^q, \rho_i^{q-1} + \eta\psi^q),$$

with respect to η and imposing $J'(0) < 0$. Following [5, 8] we prove that the choice

$$\phi^q = \mathrm{Re}\left(\frac{1}{\mathrm{meas}(\Omega_d)}\int_{\Omega_d}\sum_{\ell=-L}^{L}\nabla u_{s_\ell}\nabla p_{s_\ell}\right), \qquad \psi^q = \mathrm{Re}\left(\frac{1}{\mathrm{meas}(\Omega_d)}\int_{\Omega_d}\sum_{\ell=-L}^{L} s_\ell\, u_{s_\ell} p_{s_\ell}\right), \quad (8)$$

ensures $J'(0) < 0$. The fields u_{s_ℓ}, p_{s_ℓ} are solutions of (4) and (7), respectively, taking $\Omega = \Omega_d$, $\kappa_i = \kappa_i^{q-1}$ and $\rho_i = \rho_i^{q-1}$.

Our algorithm alternates a few gradient iterations to correct the parameters with a topological derivative evaluation to update the domains. Once the parameters are corrected, we compute again the topological derivative to update the domains, and update the current approximation by adding to the previous domain the points where the topological derivative attains now the largest negative values. Once the approximation of the domains is improved we perform further gradient iterations to update the parameters and so on. The algorithm stops when either $\mathrm{meas}(\Omega_d \setminus \Omega_{d-1})$, $|\kappa_i^q - \kappa_i^{q-1}| + |\rho_i^q - \rho_i^{q-1}|$ and $\|U_{meas} - U_{total}\|$ are small, or $J(\mathbb{R}^2_- \setminus \Omega_d, \kappa_i^q, \rho_i^q)$ is small.

When $\Omega = \cup_{j=1}^{D}\Omega_j$ and the parameters κ_i, ρ_i are piecewise constant with values $\kappa_{i,j}$, $\rho_{i,j}$ inside Ω_j, the method can be generalized as follows. Given an approximation $\Omega_d := \cup_{j=1}^{D'}\Omega_{d,j}$ (D' is not necessarily equal to the true number of defects D), the values of the parameters are updated by $\kappa_{i,j}^q = \kappa_{i,j}^{q-1} + \eta\phi_j^q$ and $\rho_{i,j}^q = \rho_{i,j}^{q-1} + \eta\psi_j^q$ with $\phi_j^q = \mathrm{Re}\left(\frac{1}{\mathrm{meas}(\Omega_{d,j})}\int_{\Omega_{d,j}}\sum_{\ell=-L}^{L}\nabla u_{s_\ell}\nabla p_{s_\ell}\right)$ and $\psi_j^q = \mathrm{Re}\left(\frac{1}{\mathrm{meas}(\Omega_{d,j})}\int_{\Omega_{d,j}}\sum_{\ell=-L}^{L} s_\ell\, u_{s_\ell} p_{s_\ell}\right)$. Now u_{s_ℓ} and p_{s_ℓ} solve (4) and (7) with $\Omega = \cup_{j=1}^{D'}\Omega_{d,j}$, and thermal parameters $\kappa_i = \kappa_{i,j}^{q-1}$ and $\rho_i = \rho_{i,j}^{q-1}$ in $\Omega_{d,j}$. The topological derivative is computed using (6) with u_{s_ℓ} and p_{s_ℓ} defined as above (considering the current piecewise constant values of the parameters). The values of κ_i, ρ_i in $\mathbb{R}^2_- \setminus \Omega_d$ are taken as the initial guesses κ_i^0, ρ_i^0.

4 Numerical example

We consider the reconstruction of two inclusions of different sizes located at different depths. To simplify computations, we assume that the conductivities of the inclusions are known and equal to the exterior one: $\kappa_e = \kappa_{i,1} = \kappa_{i,2} = 1$. In the exterior media $\rho_e = 0.2$. The unknowns of the inverse problem (represented in Fig. 2(a)) are the two defects Ω_1 and Ω_2 and the values of their densities $\rho_{i,1} = 1$ and $\rho_{i,2} = 2$. We generate 7 incident excitations at the sources represented by '•' marks in all the plots in Fig. 2. The temperature is then measured at the 8 observation points represented by '×' marks at 10 uniformly distributed times in the time interval [0.05, 0.5]. Data were generated solving the corresponding direct problem using the numerical method detailed in [3, 8] and adding a 1% gaussian relative error at each observation point.

We start the algorithm setting $\rho_i^0 = 0.5$ everywhere. The topological derivative (TD) of the functional $J(\mathbb{R}^2_-, \rho_i^0)$ at the sampling region $[-3.5, 3.5] \times [-2.5, 0]$ is represented in Fig. 2(b). The regions where the TD attains large negative values (dark blue colors on the plot) characterize the expected location of the defects. We observe that all these points are concentrated in the same region, suggesting that only one defect is buried in the medium. Notice that these points belong to the true defect Ω_2, which is the biggest and is closest to the boundary Π. Furthermore, the true value $\rho_{i,2}$ provides a higher contrast with ρ_e than $\rho_{i,1}$. The initial guess for Ω is represented in Fig. 2(c). Now we update the initial value $\rho_{i,2}^0 = 0.5$ by the gradient technique. After ten

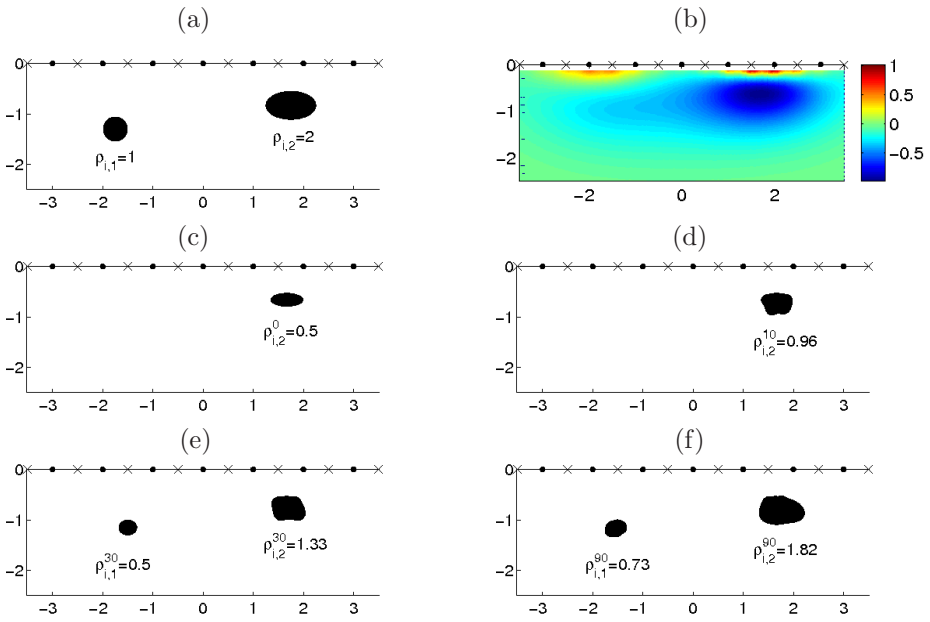

Figure 2. (a) *True configuration.* (b) *Topological derivative of* $J(\mathbb{R}^2_- \setminus \Omega, \rho_i)$ *with initial values* $\Omega^0 = \emptyset$ *and* $\rho_i^0 = 0.5$. (c) *Approximate domain* $\Omega^1_{i,2}$ $(\Omega^1_{i,1} = \emptyset)$. (d) *Approximate domain* $\Omega^2_{i,2}$ $(\Omega^2_{i,1} = \emptyset)$ *and current value of the parameter* $\rho_{i,2}$. (e) *Approximate domains* $\Omega^4_{i,1}$ *and* $\Omega^4_{i,2}$ *and current values of the parameters.* (f) *Final reconstruction after 9 iterations of the algorithm.*

iterations we obtained the value $\rho^{10}_{i,2} = 0.9644$. In the next step a new TD computation is performed, yielding the domain represented in Fig. 2(d). The algorithm continues by alternating 10 gradient iterations with a TD computation. After three TD computations the smaller defect is detected. We take then as initial guess $\rho^{30}_{i,1} = 0.5$ (the superscript 30 means that globally we have already performed 30 gradient iterations, although they only affect the approximation of $\rho_{i,2}$, which is $\rho^{30}_{i,2} = 1.3313$ at this stage). The current domains are represented in Fig. 2(e). After 9 iterations the algorithm stopped. The final reconstructed objects are given in Fig. 2(f). The estimated values of the parameters are $\rho^{90}_{i,1} = 0.7292$ and $\rho^{90}_{i,2} = 1.8227$. The overall reconstruction is quite satisfactory taking into account that few data were available, distorted by noise. It is also remarkable that we were able to characterize not only the big object, but also the smaller one, which has less contrast with the exterior and is located further from the observation/source points.

Acknowledgments

The authors are partially supported by the Spanish Government research project TRA2010–18054 and the Spanish Ministerio de Economía y Competitividad Grant No. FIS2011–222888–C02–02.

References

[1] Garrido F and Salazar A Thermal wave scattering from spheres 2004 *J. Appl. Phys.* **95** 140-149
[2] Mendioroz A, Castelo A, Celorrio R and Salazar A 2013 Characterization of vertical buried defects using lock-in vibrothermography: I. Direct problem *Meas. Sci. Technol.* **24** 065601-65611
[3] Hohage T and Sayas FJ 2005 Numerical approximation of a heat diffusion problem by boundary element methods using the Laplace transform *Numer. Math.* **102** 67-92
[4] López-Fernández M and Palencia C 2004 On the numerical inversion of the Laplace transform of certain holomorphic mappings *Appl. Numer. Math.* **51** 289-303
[5] Carpio A and Rapún ML 2008 Domain reconstruction by photothermal techniques *J. Comput. Phys.* **15** 8083-8106

[6] Carpio A and Rapún ML 2014 Parameter Identification in Photothermal Imaging *J. Math. Imaging Vis.* **49** 273-228
[7] Sokolowski J and Zolésio JP 1992 *Introduction to shape optimization. Shape Sensitivity Analysis* (Heidelberg: Springer)
[8] Carpio A and Rapún ML 2008 Solving inverse inhomogeneous problems by topological derivative methods *Inverse Problems* **24** 045014